Microchimica Acta (2022) 189:437
https://doi.org/10.1007/s00604-022-05522-z

ORIGINAL PAPER

Photothermal biosensor for HPV16 based on strand-displacement amplification and gold nanoparticles using a thermometer as readout

Bingyan Yan[1,2] · Min Li[3] · Fang Luo[2] · XiaoYa Jin[1] · Bin Qiu[2] · Zhenyu Lin[2]

Received: 7 July 2022 / Accepted: 30 September 2022

Abstract

Gold nanoparticles (AuNPs) in aggregated state have a strong near infrared region (NIR) absorption and the causes a much stronger photothermal effect than that of the dispersed AuNPs. Strand-displacement amplification (SDA) can produce large amount of single-stranded DNA (ssDNA), which in turn effectively prevent AuNPs from aggregation. In this study, these characteristics had been applied to design a photothermal biosensor for human papilloma virus (HPV and HPV16 were chosen as model target) detection. In the absence of HPV16, AuNPs was in the aggregated state and large temperature rise can be detected after the irradiation by 808 nm laser. The presence of HPV16 triggers the SDA reaction with the help of Bst DNA polymerase and Nt.BstNBI nicking endonuclease resulting in the production of large amounts of ssDNA; this protects unmodified AuNPs from salt-induced aggregation. Therefore, AuNPs was in a dispersed state and the temperature change was not significant after the irradiation of 808 nm laser. The difference of the temperature changing can be applied for the quantitative detection of HPV16 using a thermometer as readout. The linear response range is 1.0 fM ~ 50 pM with a detection limit of 0.3 fM. The proposed method has been applied to detect HPV16 in clinical cervical sample and is competent for clinical analysis.

Keywords Photothermal effect · Gold nanoparticle · Strand-displacement amplification · Human papillomavirus · Thermometer

Introduction

Thermometer is an ideal signal readout device because of its easy access, low cost, and simple operation, which had been used as readout equipment and been coupled with the photothermal effect of different reagents to design diverse biosensors [1–4]. The photothermal effects of gold nanoparticles (AuNPs) at different state change greatly [5–7]. The AuNPs in aggregated state have a strong near infrared region (NIR) absorption and result in a much stronger photothermal effect than that of the dispersed AuNPs [8, 9], leading to an increase in temperature surrounding environment. Modulating the electrostatic stability is a common method to regulate the aggregation state of AuNPs. The surface of the citrate capped AuNPs is negatively charged and it exists dispersed in solution due to electrostatic repulsion. When the salt solution is added, the negatively charged AuNPs surface is neutralized by the salt solution with the opposite charge. The inter-particle repulsion is not sufficient to stabilize the dispersion of AuNPs, resulting in their aggregation [10]. When short single-stranded DNA (ssDNA) is present,

Bingyan Yan and Min Li contributed equally to this work

✉ XiaoYa Jin
jinxy0001@163.com

✉ Zhenyu Lin
zylin@fzu.edu.cn

[1] Department of Infectious Diseases, The Key Laboratory of Diagnosis and Controlment for The Development of Chronic Liver Disease of Zhejiang Province, The First Affiliated Hospital of Wenzhou Medical University, Wenzhou 325025, China

[2] Ministry of Education Key Laboratory for Analytical Science of Food Safety and Biology, Fujian Provincial Key Laboratory of Analysis and Detection for Food Safety, College of Chemistry, Fuzhou University, 2 Xue Yuan Road, University Town Fuzhou, Fuzhou 350116, Fujian, People's Republic of China

[3] Department of General Medicine, Fujian Provincial Hospital, Provincial Clinical 13 Medical College of Fujian Medical University, Fuzhou, Fujian 350001, China

Published online: 02 November 2022

ssDNA can be adsorbed by AuNPs through van der Waals forces between its exposed bases and AuNPs, thus protecting the AuNPs from salt-induced aggregation and leaving the AuNPs in a dispersed state [11, 12]. This character has been applied to design photothermal biosensors for adenosine [13] and bifidobacteria [14]. Based on the similar principle, a photothermal assay for p53 detection of using a DNA walker for signal amplification had been designed [1]. Early study indicated that the more ssDNA produced, the better AuNPs aggregation can be prevented. In order to enhance the sensitivity of the biosensor, a signal amplification strategy which can produce large amount of ssDNAs can meet this goal.

Strand-displacement amplification (SDA) reaction is a reaction which enables rapid amplification of short ssDNA with the participation of DNA polymerase and incisional nucleic acid endonuclease [15, 16]. In a typical SDA reaction, the initiator strand hybridizes with the template strand and extends along the template strand with the help of DNA polymerase. Nucleic acid endonucleases cut the double-strand DNA (dsDNA) at the recognition site, generating a short ssDNA and an incomplete dsDNA. The DNA polymerase then extends the DNA strand in the presence of dNTPs, resulting in a new cut site. Through this cycle, a large amount of ssDNA can be produced [17, 18]. This can be applied to produce ssDNA rapidly and in large quantities, thus prevent the AuNPs from aggregation effectively and much sensitive photothermal biosensor can be developed.

Human papillomavirus (HPV) infection causes almost all cases of cervical cancer [19–21], which is easily curable if diagnosed and treated early [22]. Most cases of cervical cancer are caused by HPV16 infection [23, 24]. HPV 16 testing is part of the gold-standard for cervical cancer diagnosis [25]. The mostly used methods are Pap smear [26], fluorescent PCR methods [27], and electrochemical methods [28–30], which rely on expensive equipment and high requirements of personnel operation. It is important to construct low-cost methods for HPV16 testing in resource-limited area. Therefore, HPV16 was chosen as the model target. In this study, an accurate and low-cost photothermal method for HPV16 detection has been constructed based on SDA reaction and changes in the aggregation state of AuNPs. The presence or absence of HPV16 leads to differences in the aggregation state of AuNPs and thus cause differences photothermal response after the irradiation of 808 nm laser, which can be used to detect target easily. The propose method is simple, low cost, accurate, and suitable for low-resource environments through colorimetric-temperature dual-channel readout.

Experimental section

Reagents

All oligonucleotides and hairpin probe (HP) were synthesized by Sangon Biotechnology Co., Ltd. (Shanghai, China). The sequences are shown as follows:

HPV16: 5′-GCTGGAGGTGTATG-3′
HPV18: 5′-GGAATGCTCGAAGGTCGTCT-3′
HPV31: 5′-GGTGAACCGAAAACGGTTGG-3′
HPV51: 5′-ACCGATTTCGGTTACGCCCT-3′
HPV58: 5′-ACAGCTAGGGCACACAATGG-3′
HP: 5′-GTGTATGTTTTTGACTCGGGGGCATACACC TCCAGC-3′

The other reagents used in the experiments and the preparation of AuNPs are shown in the supplementary materials.

Production of ssDNA via SDA

The HP was first annealed at 90 °C, and slowly cooled down to 25 °C (room temperature) after 10 min. A volume of 25 μL of 1 × Tris–HCl containing 200 nM HP and HPV16 was incubated at 37 °C for 1.5 h. Then, 15 μL Tris–HCl, 0.5 μL $MgSO_4$, 2 μL of 500 μM dNTPs, 1 μL of 8 U/μL Bst DNA polymerase, 1.5 μL of 10 U/μL Nt.BstNBI nicking endonuclease, and their corresponding buffer solutions were added into the above solution and maintain at 55 °C for 1.5 h. Then, the resulting solution was heated at 80 °C for 10 min and slowly cooled down to 25 °C.

Photothermal detection of HPV16

The details of the procedures about the sample collection were shown in supplementary materials. During the photothermal detection of HPV16, the total volume of each test solution was fixed at 250 μL to ensure accurate results. A volume of 40 μL of above solution, 4 μL of Tris–HCl buffer, and 200 μl of AuNPs was mixed and shaken to mix well. Subsequently, 6 μL of 500 mM NaCl was added. The mixture was incubated at 25 °C for 5 min to achieve salt-induced aggregation of AuNPs.

Then, an 808 nm portable laser was used to irradiate the mixed solution. The power density of the continuous laser irradiation was 3 W/cm^2. The laser was in the shape of a dot. The duration of the exposure was 10 min. The mixed solution should immediately be measured by digital thermometer (CIE 305P). In all temperature measurements, the thermometer probe was positioned fixed to avoid temperature variations between positions, at a distance of 1 cm from the bottom of the detector tube. To reduce heat exchange

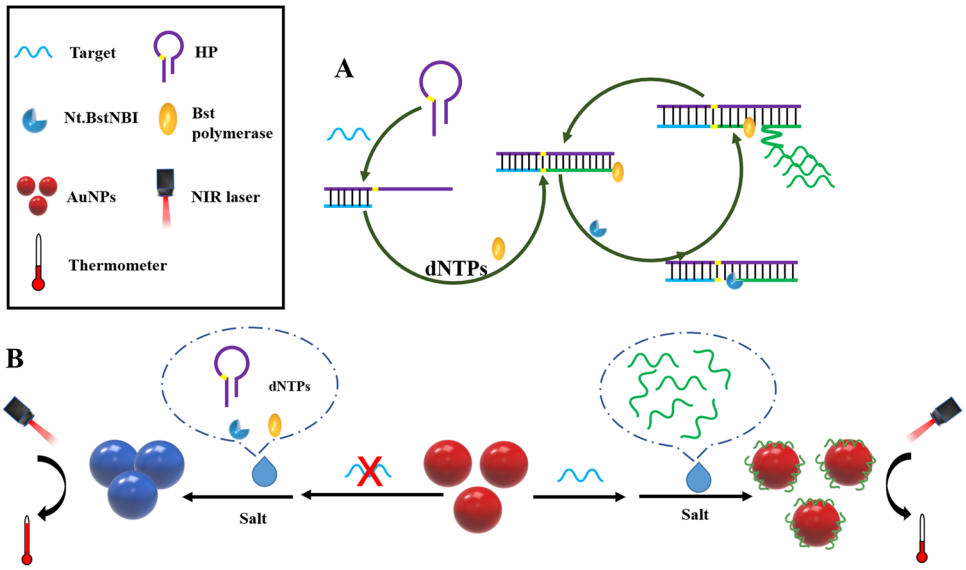

Scheme 1 Schematic illustration of the principle of HPV16 biosensor based on target-triggered SDA and prevention of gold nanoparticles aggregation using a thermometer as readout system. Route A was the process of target-triggered SDA that produces a large amount of short ssDNA. Route B was the process of photothermal detection at present and absent of targets

between the reaction solution and the environment, a foam layer was used as a heat shield around the reaction solution in all experiments.

Other experimental procedures

Experimental methods for preparation of AuNPs, polyacrylamide gel electrophoresis, fluorescence measurement, optimization of salt concentration, and real sample detection are described in detail in the Supplementary Materials.

Results and discussion

Principle of the proposed photothermal biosensor

The mechanism of the proposed photothermal method for HPV16 detection based on target-triggered SDA and prevention of AuNPs aggregation is demonstrated in Scheme 1. Nt.BstNBI is a site-specific endonuclease that cuts only one DNA strand on a dsDNA substrate. The incision endonuclease catalyzes the recognition of a specific sequence (GAGTC) with the cut site being the last 4 bases of the sequence near the 3' side. In the presence of HPV16, stem loop structure of HP was opened through the hybridization with target. With the help of dNTPs, the 3' end fragment of the opened HP can be extended as a template by the action of Bst polymerase and a dsDNA with a recognition site for Nt.BstNBI was produced. Then, Nt.BstNBI cleaves the ssDNA downstream of the recognition site and subsequently, Bst polymerase continues to replicate along the strand. After a certain point, the endonuclease stopped shearing and the chain was continuously elongated. In such a complete reaction process, a large amount of ssDNA was generated, which can be used to keep AuNPs dispersed in salt solution. Since the photothermal effect AuNPs in dispersed state is low, the temperature change of the system was not significant after the irradiation of 808 nm laser. In the absence of HPV16, the HP in the system is self-structured and can not protect the AuNPs from aggregation in the salt solution. So, large temperature rise could be detected after the irradiation of 808 nm laser. The difference of the temperature changing of the system can be applied for quantitative detection of HPV16 by using thermometer as a readout system.

Feasibility study

Polyacrylamide gel electrophoresis experiment was performed to verify the successful of the signal amplification process. As shown in Fig. 1A, lanes 1and 2 represent the target (12 bases) and HP (44 bases), respectively. The band above the lane 3 was the product of the hybridization between target and HP (56 bases). Lane 4 was the reaction system without the target, which with only the HP structure at the bottom. Because of the absence of target, the added dNTPs were not consumed at all, and the excessive dNTPs concentration led to the trailing phenomenon in lane 4. Lane 5 represents the reaction system with target HPV16. The band below the lane was an excess of HP structure (44 bases) and above was dsDNA which has been continuously elongated after the complete amplification reaction (88 bases). The short ssDNA which was cut off by Nt.BstNBI had only 8 bases and was not visible in gel electrophoresis, so it was verified by fluorescence experiments. In the presence of the target, the solution with SYBR Green II showed a strong fluorescent signal. If the target not existed, only weak fluorescence signal detected. These results verified that

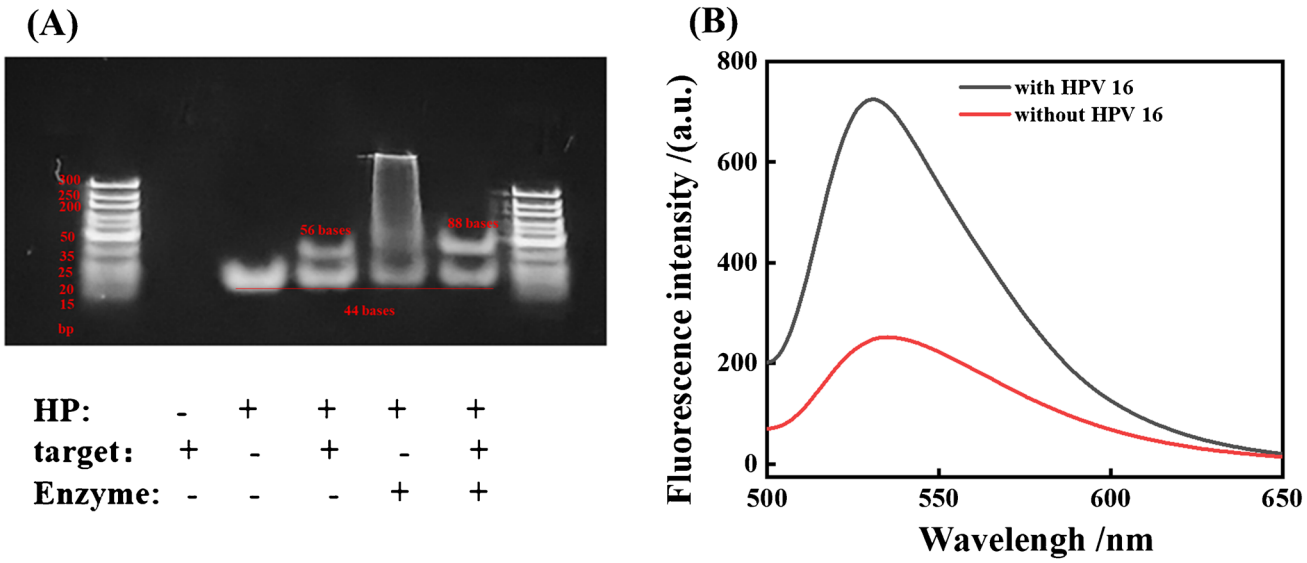

Fig. 1 **A** PAGE analysis of the products of the reaction system. **B** The fluorescence analysis of the products of the reaction system

a large amount of ssDNA was produced in the presence of the HPV16 (Fig. 1B).

The prepared AuNPs without the addition of salt solution was uniformly dispersed and the solution color was red; the readout temperature was 28.5 °C after laser irradiation, which is close to room temperature (Fig. 2A). After adding high-concentration salt solution to the system after SDA, in the absence of the target, AuNPs were in a salt-induced aggregation state and the solution color changed to colorless. The temperature was 52.3 °C after laser irradiation (Fig. 2B). When abundant HPV16 existed, a large amount of short ssDNA, which protected AuNPs from salt-induced aggregation, presents a dispersed state. The temperature was 30.4 °C, close to the dispersed pure AuNPs (Fig. 2C).

The temperature response induced by the target was further confirmed in Fig. 2D. In the absence of the target, the value of temperature increase under laser irradiation could reach about 26 °C (curve a). When 100 fM target exists, the digestion cycle was triggered by HPV16 and the system amplified much ssDNA which protects the dispersion of AuNPs. The value of temperature increase was about 19 °C (curve b). The 50 pM target led to more ssDNA products with a temperature change around 5 °C (curve c), close to the temperature increase of uniformly dispersed pure AuNPs (curve d).

The mechanism of this phenomenon was further investigated using UV–vis spectra (Fig. 2E). According to previous reports, there is a large temperature change of AuNPs when the surface plasmon resonance (SPR) absorption peak is close to the wavelength of the illumination laser, which is the reason for the significant enhancement of the photothermal effect of the aggregated AuNPs under 808 nm laser irradiation. The maximum absorption peak of AuNPs was located at 520 nm in the UV–vis spectrum (curve d). Upon the addition of NaCl, the absorption peak at 520 nm disappeared and the absorption at 808 nm was enhanced, which was due to salt-induced aggregation of AuNPs (curve a). With the addition of 100 fM target, the absorption at 808 nm was weaker than curve a, so the temperature increase was not as pronounced as no target (curve b). In the presence of the 50 pM HPV16, the peak shape was similar to the pure AuNPs. Therefore, there was almost no increase in temperature under laser irradiation (curve c). All these results verified the feasibility of the proposed biosensor.

Optimization of the reaction conditions

The optimum conditions for HPV16 assay were achieved via adjusting some parameters, that is, the concentration of salt solution, the concentration of Bst polymerase, the hybridization time between the target and HP structure, the digestion time, reaction pH, and reaction temperature. For detailed optimization results, refer to Figure S1 in the supplementary materials. The salt concentration of 120 mM, Bst polymerase concentration of 300 U/mL, hybridization time of 1.5 h, incubation time of 1.5 h, pH of 8.0, and temperature of 55 °C were determined as the optimal reaction conditions. The performance of the method was examined under optimal experimental conditions.

Performance of the proposed method

As shown in Fig. 3A, ΔT (the difference of the temperature at absent and present of target) increased with increasing

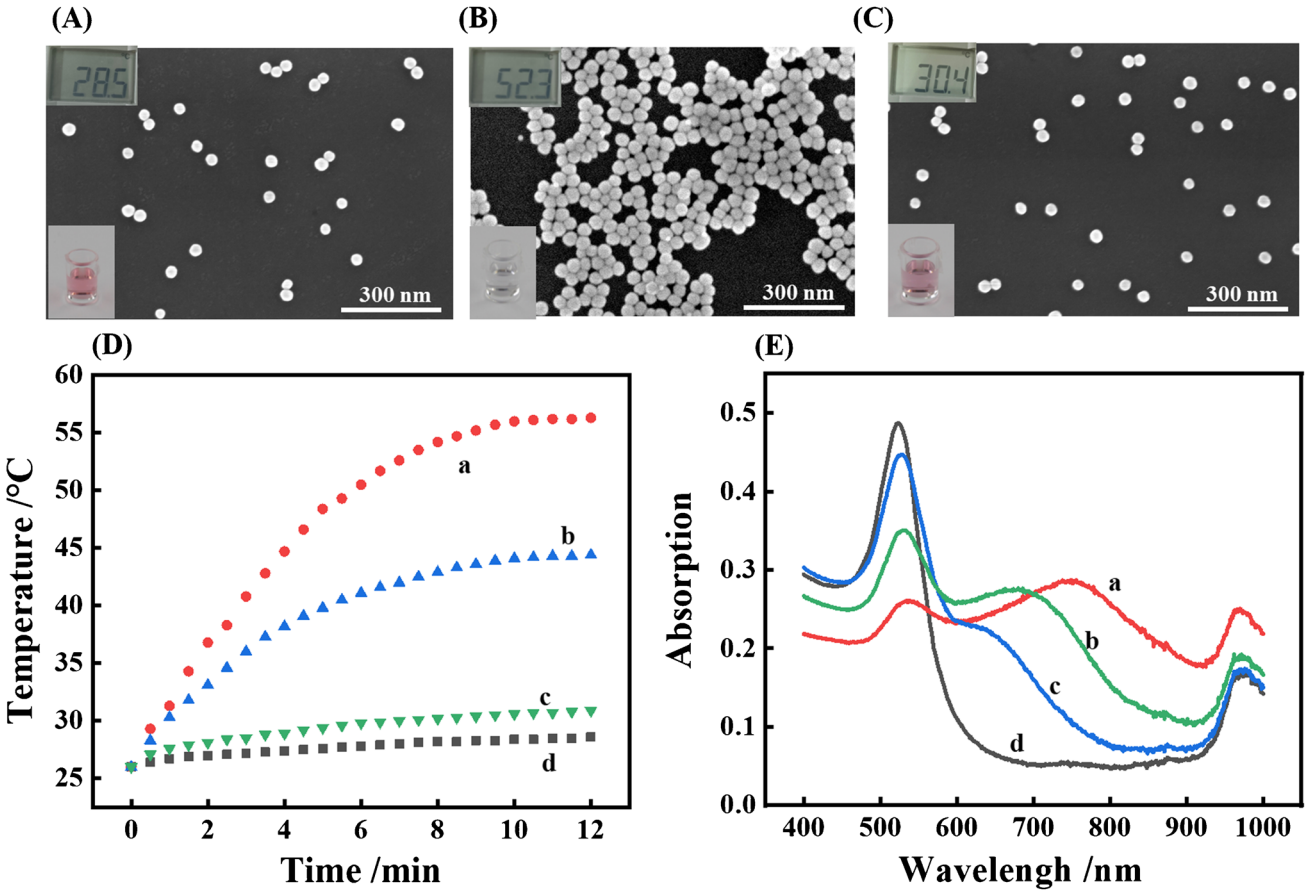

Fig. 2 SEM images of **A** pure AuNPs without the addition of salt solution, **B**–**C** AuNPs mixed with salt solution and different SDA products, **B** without HPV16 and **C** with HPV16. Insets were the photographs of the corresponding temperature indication (upper left) and samples (bottom left) after laser irradiation. **D** Temperature comparison among (a) without HPV16 (aggregated AuNPs), (b) with 100 fM HPV16, (c) with 50 pM HPV16, and (d) pure AuNPs without the addition of salt solution. **E** UV–vis absorption spectra comparison (a) without HPV16 (aggregated AuNPs), (b) with 100 fM HPV16, (c) with 50 pM HPV16, and (d) pure AuNPs without the addition of salt solution

HPV16 concentration. The results show that the logarithm of HPV16 concentration has a linear relationship with ΔT in the range of 1.0 fM ~ 50 pM (Fig. 3B). The linear equation can be expressed as follow:

$$\Delta T = 4.08 logC + 16.30 \left(R^2 = 0.9973\right)$$

where C was HPV16 concentration and R was the correlation coefficient. The calculated limit of detection (LOD) was 0.3 fM (LOD = 3 s/k). Actual minimal quantity of detection in moles was 7.5×10^{-12} mol. The inset was photographs of the samples with different concentrations of the target. There was a relatively obvious difference in their colors, so colorimetry could also be used as a readout method. But since the color of the solutions had little difference under low target concentrations, the detection limit of the colorimetric method is not as low as that of the proposed method, and a spectrometer was still required for accurate quantification.

In order to compare the experimental results, we also performed UV–vis absorption spectra analysis. As shown in Fig. 3C, the absorption at 520 nm was positively correlated with HPV16 concentration. The background error could be reduced by using the absorbance ratio (the absorbance at 520 nm with HPV16 to the absorbance at 520 nm without HPV16). Absorbance ratio at 520 nm and the logarithm of HPV16 concentration were linear in the range from 10 fM to 25 pM (Fig. 3D). The linear equation can be expressed as follow:

$$Y = 1.50 logC + 0.26 \left(R^2 = 0.9958\right)$$

where Y, C, and R were the absorbance ratio at 520 nm, HPV16 concentration, and the correlation coefficient, respectively.

In contrast to the use of spectral readout, the use of a thermometer as a readout system had lower detection

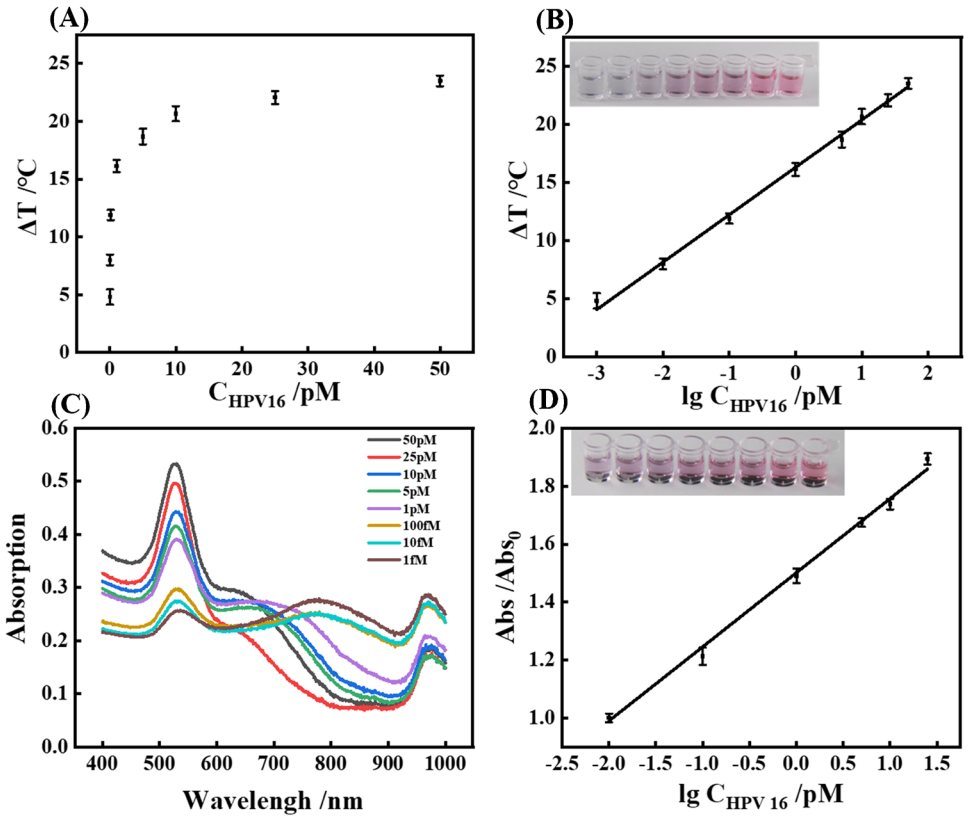

Fig. 3 **A** Plot of the ΔT versus the concentration of HPV16. **B** The linear relationship between ΔT and logarithm of HPV16 concentration. The inset is the photograph of the samples after laser irradiation. **C** UV–vis absorption spectra comparison under different HPV16 concentration. **D** The linear relationship between the absorption ratio and logarithm of HPV16 concentration. The inset is the photograph of the samples before laser irradiation

limit, larger detection range, and did not require expensive laboratory instrumentation. By combining a simple signal amplification strategy, the detection limit of this method was much lower than that of other colorimetric methods and comparable to the electrochemiluminescence (ECL) detection technologies. Furthermore, our method has the advantage of less time-consuming (shown in Table 1).

The selectivity of the system was evaluated using HPV18, HPV31, HPV51, and HPV58 as potential interferences. Figure 4 shows the ΔT after reaction with HPV16 (1 pM) and other HPV sequences (1 nM). In the presence of 1 pM HPV16, the ΔT was about 16.3℃. In contrast, when other HPV sequences of 1 nM exist, all the ΔTs were less than 3℃, which were close to the blank value. Only HPV16 could trigger the SDA, confirming the good selectivity of the experiment.

Determination of HPV16 in clinical cervical sample

To further evaluate the application of the method, we applied the method to detect HPV16 in human cervical brush samples. The cervical brush samples from patients in the First Affiliated Hospital of Xiamen University were used in this experiment. Details of the processing can be found in Supplementary Materials. Four negative samples (1–4) and six positive samples (5–10) were tested. Each sample was divided into three groups for measurement, taken the average number of measurement results as the reference

Table 1 Comparison of analytical performance of different methods for HPV detection

Detection methods	Sample	sample volume	Turn-around time	LOD	Linear range	Ref
ECL	Clinical samples	120 μL	6 h	1.41 aM	0.1fM–5 pM	Lu et al. (2022) [31]
ECL	Cancer cell lines	300 μL	4.5 h	6.8 aM	10 aM–10 nM	Hong et al. (2021) [32]
ECL	–	–	4 h	0.03 nM	0.1–200 nM	Nie et al. (2020) [33]
ECL	Clinical samples	100 μL	5 h	7.6 fM	0.01–15 pM	He et al. (2021) [34]
ECL	Clinical samples	–	4.75 h	0.1 fM	1fM–50 pM	He et al. (2020) [35]
Colorimetric	Clinical samples	250 μL	3 h	3.3 fM	10 fM–25 pM	This work
Photothermal	Clinical samples	250 μL	3 h	0.3 fM	1fM–50 pM	This work

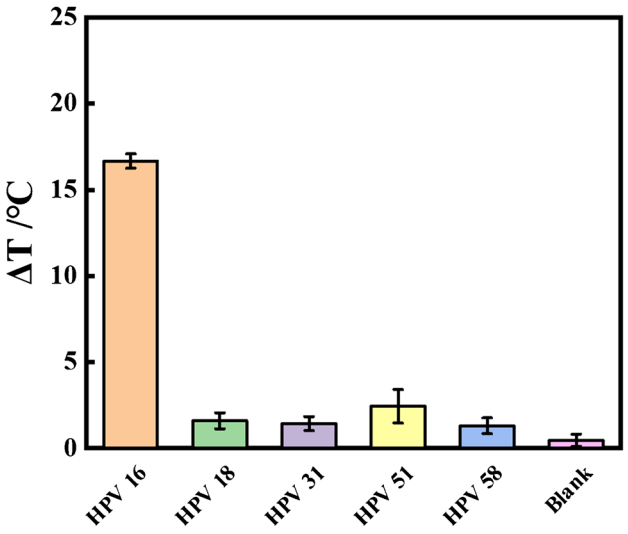

Fig. 4 Selectivity of the proposed method for HPV16 detection. HPV16 used was 1.0 pM. The concentration of other interferents was 1.0 nM

consequence. The experimental results are shown in Table 2. The recovery rate ranged from 99.7 to 110.2%, and the relative standard deviation (RSD) was 1.7 ~ 4.1%. These results suggest that the proposed photothermal method can be applied to detect targets in clinical samples.

Conclusion

A simple, low-cost method for the detection of HPV16 has been developed based on SDA and the difference of AuNPs aggregation-induced photothermal effects. The method uses both color change and temperature change as dual signal outputs, offering the advantage of high specificity and a simple and accurate readout. By designing different DNA structures, the method can be extended to detect other different targets, thus broadening the range of applications for sensors with a thermometer as the readout

Table 2 Application of the method to detect HPV16 DNA in clinical samples ($n = 3$)

Sample	Detected (fM)	Added (fM)	Total Found (fM)	Recovery (%)	RSD (%)
sample 1	0.5	0	0.5	-	3.0
		10	10.7	102.0	3.7
		100	100.2	99.7	2.6
sample 2	0.7	0	0.7	-	1.7
		10	10.9	102.0	2.8
		100	100.6	99.9	2.7
sample 3	0.4	0	0.4	-	3.5
		10	10.6	102.0	3.7
		100	100.1	99.7	2.4
sample 4	0.7	0	0.7	-	3.4
		10	11	103.0	2.2
		100	101.2	100.5	1.9
Sample 5	73.6	0	73.6	-	3.4
		10	84.3	107.0	2.4
		100	180.5	106.9	2.0
Sample 6	65.0	0	65.0	-	3.3
		10	75.9	109.0	3.2
		100	170.2	105.2	2.6
Sample 7	59.7	0	59.7	-	3.1
		10	70.2	105.0	3.3
		100	166.3	106.6	4.0
Sample 8	67.5	0	128.2	-	3.6
		10	138.6	104.0	4.1
		100	236.1	107.9	2.8
Sample 9	92.1	0	92.1	-	2.5
		10	102.8	107.0	3.4
		100	195.5	103.4	4.2
Sample 10	85.0	0	85.6	-	2.7
		10	95.4	98.0	3.1
		100	195.8	110.2	3.9

system. The method has been applied to clinical samples and is consistent with clinical results.

Supplementary Information The online version contains supplementary material available at https://doi.org/10.1007/s00604-022-05522-z.

Author contribution The manuscript was written through contributions of all authors. B.Y., M.L., and Z.L. conceived the projects, and B.Y., M.L., F.L., X.J., and Z.L. designed and performed the experiments and collected the data. B.Y., M.L., F.L., X.J., B.Q., and Z.L. analyzed and discussed the data. All authors discussed the results and contributed to the writing of this manuscript. All authors have given approval to the final version of the manuscript.

Funding This project was supported by the National Sciences Foundation of China (21904020, 21974020), Health Science and Technology Project of Zhejiang Province (2022KY887).

Declarations

Conflict of interest The authors declare no competing interests.

References

1. Tao Y, Wang W, Fu C, Luo F, Guo L, Qiu B, Lin Z (2020) Sensitive biosensor for p53 DNA sequence based on the photothermal effect of gold nanoparticles and the signal amplification of locked nucleic acid functionalized DNA walkers using a thermometer as readout. Talanta 220:121398. https://doi.org/10.1016/j.talanta.2020.121398
2. Tao Y, Lin Y, Luo F, Fu C, Lin C, He Y, Cai Z, Qiu B, Lin Z (2021) Convenient detection of h2s based on the photothermal effect of Au@Ag nanocubes using a handheld thermometer as readout. Anal Chim Acta 1149:338211. https://doi.org/10.1016/j.aca.2021.338211
3. Zhang J, Xing H, Lu Y (2018) Translating molecular detections into a simple temperature test using a target-responsive smart thermometer. Chem Sci 9(16):3906–3910. https://doi.org/10.1039/C7SC05325H
4. Zhou W, Sun J, Li X (2020) Low-cost quantitative photothermal genetic detection of pathogens on a paper hybrid device using a thermometer. Anal Chem 92(21):14830–14837. https://doi.org/10.1021/acs.analchem.0c03700
5. Chen H, Shao L, Ming T, Sun Z, Zhao C, Yang B, Wang J (2010) Understanding the photothermal conversion efficiency of gold nanocrystals. Small 6(20):2272–2280. https://doi.org/10.1002/smll.201001109
6. Shi D, Sheng F, Zhang X, Wang G (2018) Gold nanoparticle aggregation: colorimetric detection of the interactions between avidin and biotin. Talanta 185:106–112. https://doi.org/10.1016/j.talanta.2018.02.102
7. Jiang Y, Shi M, Liu Y, Wan S, Cui C, Zhang L, Tan W (2017) Aptamer/AuNP biosensor for colorimetric profiling of exosomal proteins. Angew Chem Int Ed Engl 56(39):11916–11920. https://doi.org/10.1002/anie.201703807
8. Cheng X, Sun R, Yin L, Chai Z, Shi H, Gao M (2017) Light-triggered assembly of gold nanoparticles for photothermal therapy and photoacoustic imaging of tumors in vivo. Adv Mater 29(6):1604894. https://doi.org/10.1002/adma.201604894
9. Vankayala R, Hwang KC (2018) Near-infrared-light-activatable nanomaterial-mediated phototheranostic nanomedicines: an emerging paradigm for cancer treatment. Adv Mater 30(23):1706320. https://doi.org/10.1002/adma.201706320
10. Aldewachi H, Chalati T, Woodroofe MN, Bricklebank N, Sharrack B, Gardiner P (2018) Gold nanoparticle-based colorimetric biosensors. Nanoscale 10(1):18–33. https://doi.org/10.1039/C7NR06367A
11. Shahdordizadeh M, Yazdian-Robati R, Ansari N, Ramezani M, Abnous K, Taghdisi SM (2018) An aptamer-based colorimetric lead(ii) assay based on the use of gold nanoparticles modified with dsDNA and exonuclease I. Microchim Acta 185(2):151. https://doi.org/10.1007/s00604-018-2699-4
12. Zhang J, Wang L, Pan D, Song S, Boey FYC, Zhang H, Fan C (2008) Visual cocaine detection with gold nanoparticles and rationally engineered aptamer structures. Small 4(8):1196–1200. https://doi.org/10.1002/smll.200800057
13. Tao Y, Luo F, Guo L, Qiu B, Lin Z (2020) Target-triggered aggregation of gold nanoparticles for photothermal quantitative detection of adenosine using a thermometer as readout. Anal Chim Acta 1110:151–157. https://doi.org/10.1016/j.aca.2020.03.023
14. Zhou W, Hu K, Kwee S, Tang L, Wang Z, Xia J, Li X (2020) Gold nanoparticle aggregation-induced quantitative photothermal biosensing using a thermometer: a simple and universal biosensing platform. Anal Chem 92(3):2739–2747. https://doi.org/10.1021/acs.analchem.9b04996
15. Miao P, Tang Y (2020) Dumbbell hybridization chain reaction based electrochemical biosensor for ultrasensitive detection of exosomal miRNA. Anal Chem 92(17):12026–12032. https://doi.org/10.1021/acs.analchem.0c02654
16. Guo Q, Yu Y, Zhang H, Cai C, Shen Q (2020) Electrochemical sensing of exosomal microRNA based on hybridization chain reaction signal amplification with reduced false-positive signals. Anal Chem 92(7):5302–5310. https://doi.org/10.1021/acs.analchem.9b05849
17. Chen H-L, Guo M-M, Tang H, Wu Z, Tang L-J, Yu R-Q, Jiang J-H (2015) Nucleic acid amplification-based methods for microRNA detection. Anal Methods 7(6):2258–2263. https://doi.org/10.1039/C4AY02938K
18. Chen A, Gui G-F, Zhuo Y, Chai Y-Q, Xiang Y, Yuan R (2015) Signal-off electrochemiluminescence biosensor based on phi29 DNA polymerase mediated strand displacement amplification for microRNA detection. Anal Chem 87(12):6328–6334. https://doi.org/10.1021/acs.analchem.5b01168
19. Bray F, Ferlay J, Soerjomataram I, Siegel RL, Torre LA, Jemal A (2018) Global cancer statistics 2018: GLOBOCAN estimates of incidence and mortality worldwide for 36 cancers in 185 countries. CA: A Cancer Journal for Clinicians 68(6):394–424. https://doi.org/10.3322/caac.21492
20. Steenbergen RDM, Snijders PJF, Heideman DAM, Meijer CJLM (2014) Clinical implications of (epi)genetic changes in HPV-induced cervical precancerous lesions. Nat Rev Cancer 14(6):395–405. https://doi.org/10.1038/nrc3728
21. Walboomers JMM, Jacobs MV, Manos MM, Bosch FX, Kummer JA, Shah KV, Snijders PJF, Peto J, Meijer CJLM, Muñoz N (1999) Human papillomavirus is a necessary cause of invasive cervical cancer worldwide. J Pathol 189(1):12–19. https://doi.org/10.1002/(SICI)1096-9896(199909)189:1%3c12::AID-PATH431%3e3.0.CO;2-F
22. Rodriguez NM, Wong WS, Liu L, Dewar R, Klapperich CM (2016) A fully integrated paperfluidic molecular diagnostic chip for the extraction, amplification, and detection of nucleic acids from clinical samples. Lab Chip 16(4):753–763. https://doi.org/10.1039/C5LC01392E
23. Zhao X, Wu Q, Wang X, Fu Y, Zhang X, Tian X, Cheng B, Lu B, Yu X, Lan S, Lu W, Ma D, Cheng X, Xie X (2018) The performance of human papillomavirus DNA detection with type 16/18

genotyping by hybrid capture in primary test of cervical cancer screening: a cross-sectional study in 10,669 Chinese women. Clin Microbiol Infect 24(12):1322–1327. https://doi.org/10.1016/j.cmi.2018.02.027
24. Wang CC, Palefsky JM (2016) Human papillomavirus-related oropharyngeal cancer in the HIV-infected population. Oral Dis 22(S1):98–106. https://doi.org/10.1111/odi.12365
25. Zamani M, Robson JM, Fan A, Bono MS, Furst AL, Klapperich CM (2021) Electrochemical strategy for low-cost viral detection. ACS Cent Sci 7(6):963–972. https://doi.org/10.1021/acscentsci.1c00186
26. Beerens E, Van Renterghem L, Praet M, Sturtewagen Y, Weyers S, Temmerman M, Depypere H, Claeys P, Cuvelier CA (2005) Human papillomavirus DNA detection in women with primary abnormal cytology of the cervix: prevalence and distribution of HPV genotypes. Cytopathology 16(4):199–205. https://doi.org/10.1111/j.1365-2303.2005.00266.x
27. Weichert W, Schewe C, Denkert C, Morawietz L, Dietel M, Petersen I (2009) Molecular hpv typing as a diagnostic tool to discriminate primary from metastatic squamous cell carcinoma of the lung. The American Journal of Surgical Pathology 33 (4)
28. Avelino KYPS, Oliveira LS, Lucena-Silva N, Andrade CAS, Oliveira MDL (2021) Flexible sensor based on conducting polymer and gold nanoparticles for electrochemical screening of hpv families in cervical specimens. Talanta 226:122118. https://doi.org/10.1016/j.talanta.2021.122118
29. Civit L, Fragoso A, O'Sullivan CK (2010) Electrochemical biosensor for the multiplexed detection of human papillomavirus genes. Biosens Bioelectron 26(4):1684–1687. https://doi.org/10.1016/j.bios.2010.06.072
30. Civit L, Fragoso A, Hölters S, Dürst M, O'Sullivan CK (2012) Electrochemical genosensor array for the simultaneous detection of multiple high-risk human papillomavirus sequences in clinical samples. Anal Chim Acta 715:93–98. https://doi.org/10.1016/j.aca.2011.12.009
31. Lu Y, Rong X, Wu P, Shou J, Chen L, Luo F, Lin C, Wang J, Qiu B, Lin Z (2022) Sensitive electrochemiluminescence biosensor based on the target trigger difference of the electrostatic interaction between an ecl reporter and the electrode surface. Anal Chem 94(15):5823–5829. https://doi.org/10.1021/acs.analchem.1c05258
32. Hong G, Zou Z, Huang Z, Deng H, Chen W, Peng H (2021) Split-type electrochemiluminescent gene assay platform based on gold nanocluster probe for human papillomavirus diagnosis. Biosens Bioelectron 178:113044. https://doi.org/10.1016/j.bios.2021.113044
33. Nie Y, Zhang X, Zhang Q, Liang Z, Ma Q, Su X (2020) A novel high efficient electrochemiluminescence sensor based on reductive cu(i) particles catalyzed zn-doped mos2 qds for hpv 16 DNA determination. Biosens Bioelectron 160:112217. https://doi.org/10.1016/j.bios.2020.112217
34. He Y, Liu Y, Cheng L, Yang Y, Qiu B, Guo L, Wang Y, Lin Z, Hong G (2021) Highly reproducible and sensitive electrochemiluminescence biosensors for hpv detection based on bovine serum albumin carrier platforms and hyperbranched rolling circle amplification. ACS Appl Mater Interfaces 13(1):298–305. https://doi.org/10.1021/acsami.0c20742
35. He Y, Cheng L, Yang Y, Chen P, Qiu B, Guo L, Wang Y, Lin Z, Hong G (2020) Label-free homogeneous electrochemical biosensor for hpv DNA based on entropy-driven target recycling and hyperbranched rolling circle amplification. Sens Actuators, B Chem 320:128407. https://doi.org/10.1016/j.snb.2020.128407